HIGH-FREQUENCY RADAR OBSERVATIONS OF SEA WAVES TRAVELLING IN OPPOSITION TO THE WIND

DOUGLASS D. CROMBIE

Institute for Telecommunication Sciences, Office of Telecommunications, U.S. Department of Commerce, Boulder, Colorado 80302 U.S.A.

and

KLAUS HASSELMANN and WOLFGANG SELL

Max-Planck-Institute of Meteorology, Hamburg, Germany

(Received 26 September, 1977)

Abstract. High-frequency (HF) radar observations of sea waves apparently travelling against the wind are discussed. In some cases, it appears that the wave angular spectrum does contain components travelling against the wind. Some data taken on the Barbados Island during BOMEX have been analyzed, and they show that such components increase in amplitude with distance from a windward shore. It is shown that the order of magnitude of the observed growth rates can be explained by resonant non-linear interaction within the wave spectrum.

1. Introduction

HF radar observations of signals backscattered from the surface of the sea usually show the presence of waves which are both approaching and receding, as illustrated in Figure 1. In many cases, when using an omni-directional radar antenna situated on a long shore line, with an on-shore wind, the presence of approaching and receding waves arises from the geometry of the experiment. Figure 2 shows schematically the relationship between direction of the wind, the direction and magnitude of the waves causing backscatter, and the location from which backscatter is observed. Three wind directions are used for illustration, and it is assumed that the wind generates waves travelling only within 90° of the wind direction. The first is for a wind blowing perpendicularly towards the shore line. For each of the three backscatter locations, A, B, C, illustrated, the wind-generated waves have components travelling towards the radar. Backscatter from all three locations will have a positive Doppler shift. For the second wind direction (at about 45° towards the shore line), strong backscatter would be expected from location D, with much weaker backscatter from location E. In both cases the backscatter will have a positive Doppler shift. For wind direction 3 (parallel to the shore line), the situation is different. From location F, strong signals with a positive Doppler shift will be observed. From location G, equally strong signals, but with negative Doppler shifts, will be observed. Backscatter from location A with a cross-wind would not be observed. Thus the observation of receding waves when the wind is blowing towards the radar is not unexpected when the antenna has a broad beam-width and the wind direction has a component parallel to the shore line, even if it is assumed that wind generates waves travelling only within ±90° of its direction.

Boundary-Layer Meteorology **13** (1978) 45–54. *All Rights Reserved*
Copyright © 1978 by D. Reidel Publishing Company, Dordrecht, Holland

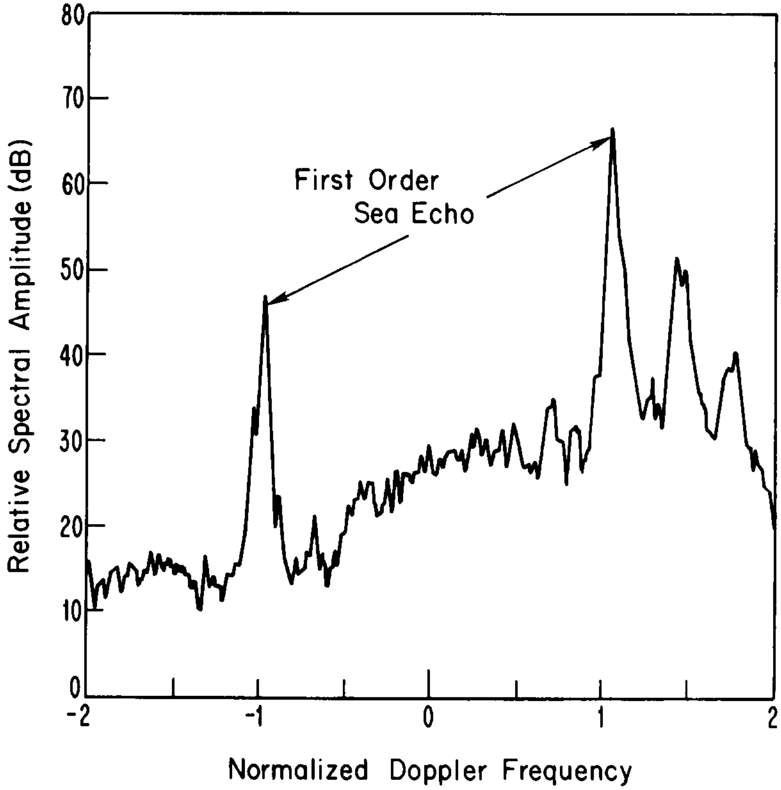

Fig. 1. Example of a radar sea-echo Doppler spectrum at 9.4 MHz. If the carrier were observed, it would appear at the center of the abcissa with ±1 corresponding to Doppler shifts ±0.313 Hz from the carrier (after Barrick *et al.*, 1974).

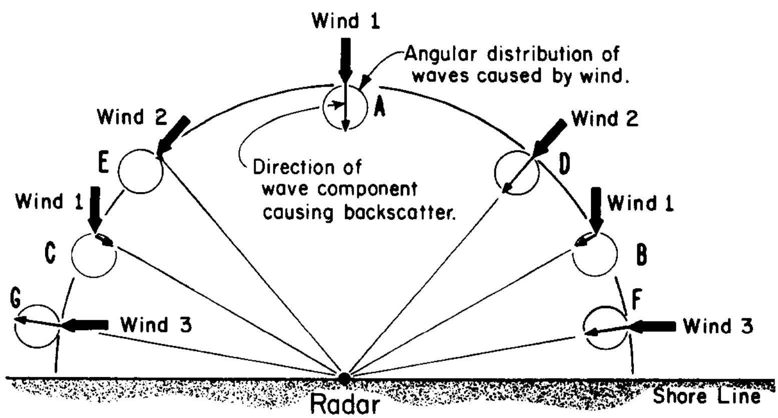

Fig. 2. Origin of apparently receding waves with a variable wind direction.

There are a few cases reported in which the azimuthal distribution of the scattered energy has been measured. One such case (Tyler *et al.*, 1974), using a moving antenna to synthesize a large antenna aperture with high directivity, showed that the angular spectrum of the waves had a width exceeding 180°. In another instance, Crombie (1972) and his colleagues used the coherence functions of signals received on two spatially separated antennas to determine the angular distribution of signals scattered by waves in the area of the Gulf stream. Because of the Gulf stream, the waves of resonant length in various directions had different phase velocities and produced varying Doppler shifts, preserving the coherence of the scattered signals. This experiment showed that signals having both positive and negative Doppler shifts were received over a continuous wide range of identical azimuthal angles. Of special interest was the presence of negative Doppler shifts even from the (approaching) wind direction.

These results, and other more frequently obtained results from simpler back-scatter techniques (Crombie, 1971), in which it is certain that the wind is blowing perpendicular to the shore line, suggest rather strongly that there are frequently components of the wind generated waves which are travelling against the wind. That is, the angular spectrum of wind generated waves has a width exceeding 180°, centered on the wind direction. In his analysis of surface pressure and wave-height correlations using an array of sensors, Snyder (1974) has similarly inferred the existence of upwind propagating waves.

The purpose of this paper is to report some observations which support these conclusions and to discuss them in terms of non-linear interactions (Phillips, 1960; Longuet-Higgins, 1962; Hasselmann, 1962, 1963a, b) between wave components generated directly by the wind.

2. Observations of Growth of Waves Travelling Against the Wind

Ground-wave high-frequency radar observations of signals backscattered by the sea off the east coast of Barbados were made during the Barbados Oceanographic and Meteorological Experiment (BOMEX) during July 1969. The equipment has been discussed adequately elsewhere (Crombie, 1971). The observations were made simultaneously at several frequencies and ranges during a two-week period. During the period of the observations, wind speeds of between 4 and 11 m s^{-1} were observed at ships mostly located about 100–200 km upwind of Barbados. Non-directional antennas were used, but the configuration of the coast line was such that the effective coverage of the antennas over the sea was somewhat less than 180°. The direction of the prevailing trade wind was towards the shore and essentially perpendicular to the coast line, leading to conditions similar to those for wind direction one in Figure 2. Thus it is believed that the observed receding waves were in fact travelling generally against the wind, rather than arising through some of the other configurations shown in Figure 2.

Although observations were made on several frequencies, the quality of those at 2.9 MHz was better than those at higher frequencies. Thus these observations (which correspond to a sea wavelength of 52 m) are discussed in detail.

The observations were made simultaneously at four ranges: 22.5, 45, 67.5, and 90 km. Each observation lasted 30 min and yielded data of the form shown in

Figure 1. The ratio of the received power at the resonant lines for negative (P_-) and positive (P_+) Doppler shifts was calculated at each of the four ranges, as shown in Figure 3. The scatter shown in Figure 3 possibly arises from differences in wind velocity during the individual measurements (8–11 m s^{-1}: 5 cases; 6–8 m s^{-1}: 4 cases; 4–6 m s^{-1}: 3 cases). But no correlation of growth rate with wind speed was observed.

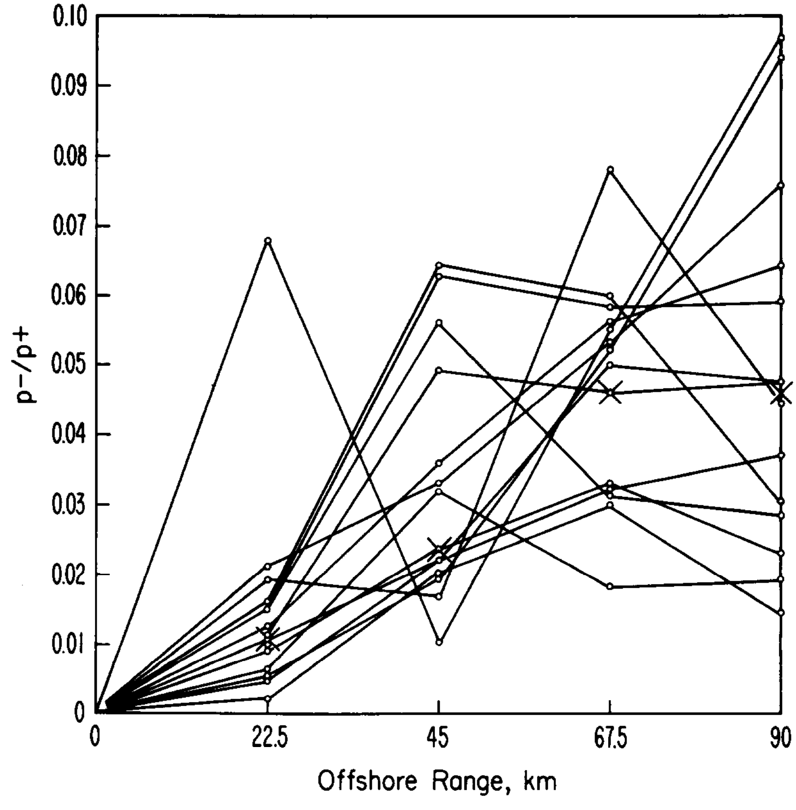

Fig. 3. Plot of the ratio of the power in receding waves to the power in approaching waves as a function of distance (frequency 2.9 MHz; sea wavelength = 52 m; median values are denoted by ×).

The signals having positive Doppler shifts arise from waves generated with an essentially infinite fetch and are thus fully developed. It is legitimate to assume that the scattering cross-section of these waves would be independent of distance over the small range of distances used. Thus the ratios shown in Figure 3 should reflect the changes in the magnitude of the receding waves. Since the P_+ and P_- observations at the different ranges were made simultaneously, many experimental errors which might otherwise occur are eliminated.

The data show a general increase with range of the power in the receding waves up to a distance of 90 km, the maximum range, although there is substantial scatter in the individual measurement. At a range of 22.5 km, the ratio P_-/P_+ varies between a minimum of 0.002 and a maximum of 0.07, with a median value of 0.01. The points representing the approximate median value of the ratio P_-/P_+ at each range show evidence of saturation between 67.5 and 90 km, which can be interpreted as a reduction in the growth rate of the receding wave at these distances.

The data for the higher frequencies (up to 7.4 MHz, corresponding to a sea wavelength of 23 m), although of lesser quality, show a generally similar growth except that the onset of saturation appears to occur at 45 km.

The data suggest rather strongly that the sea waves causing the signals with negative Doppler shifts are increasing in amplitude with distance from the shore; that is, in the upwind direction. This disposes of the possibility that the receding waves are a result of reflection of the approaching waves from the island. If such were the case, one could expect that the amplitude of the receding waves would be constant, or decrease with distance. Similarly, if the receding waves were generated directly by the wind, it might be expected that their amplitude would be independent of distance.

One other possibility should be mentioned. That is, the radar was observing waves from beyond the sheltered side of the island. However, the distance to the sheltered side (in the downwind direction) is about 25 km. At this distance, wave growth in the island's shadow would just be starting, whereas Figure 3 shows that the growth is already established at that distance. Furthermore, the ground wave attenuation ($\approx$20 dB, one way) over the island would reduce the signals scattered from the sea downwind of the island to negligible proportions.

Another possibility is that the receding waves are being generated as a result of third-order non-linear interaction between the wind generated approaching waves. This is discussed in the next section.

3. Generation of Waves Travelling Against the Wind by Wave–Wave Interactions

The energy transfer within a gravity-wave spectrum due to resonant non-linear wave–wave interactions is given by a three-dimensional Boltzmann integral (Hasselmann, 1962). The integral has been computed numerically for a number of spectral forms (Hasselmann, 1963; Hasselmann *et al.*, 1973; Cartwright, unpublished; Sell and Hasselmann, 1972; Webb, 1977), and analytically for the limiting case of an infinitely sharp spectrum (Longuet-Higgins, 1975; Fox, 1976; Herterich and Hasselman, 1977). In most of these cases, however, the energy transfer to waves travelling in the upwind direction was not presented in detail, as it was found to be far smaller than the energy transfer among components propagating in the downwind direction, which was of more immediate interest for the problem of the evolution of the spectrum (nor can upwind travelling waves be treated by the analytical sharp-peak approximation). New computations were therefore carried out for the present experiment with particular emphasis on the sea-wave energy scattered in the upwind direction.

The evolution of the two-dimensional wave spectral density $F(f, \theta; \mathbf{x}, t)$ with respect to frequency f and propagation direction θ is governed by a transport (radiative transfer) equation, which in the absence of refraction takes the form

$$\frac{\partial F}{\partial t} + \mathbf{v} \cdot \nabla F = S$$

where $\mathbf{v}$ is the group velocity and the source function S represents the net rate of change of the spectral density due to energy input, loss, and transfer processes. We shall consider only the energy transfer due to conservative non-linear interactions, so that S is identical here with the Boltzmann scattering integral.

In the configuration described in Section 2, the radar measures the two integrated quantities

$$P_{\pm}(f, r, t) = T(r) \int_{-\pi/2}^{+\pi/2} F(f, \pm\theta; \mathbf{x}(\theta), t) r \, \mathrm{d}\theta \equiv T \cdot F_{\pm}$$

where $\mathbf{x}(\theta) = (r \cos \theta, r \sin \theta)$ is the locus of points on a half-circle of radius r from the radar station and $T(r)$ denotes a transmission factor, which for an isotropically radiating antenna depends only on r. Integration of the two-dimensional transport equation over all angles within a half-plane, with $\mathbf{x} = \mathbf{x}(\theta)$ on a given half-circle, yields the equation

$$\frac{\partial P_{\pm}}{\partial t} + T \cdot v \cdot \frac{\partial}{\partial r}\left(\frac{1}{T} P_{\pm}\right) = TS_{\pm}$$

for the rate of change of the upwind or downwind half-plane spectral densities, where

$$S_{\pm} = \int_{-\pi/2}^{\pi/2} S(f, \pm\theta; \mathbf{x}(\theta), t) \, \mathrm{d}\theta.$$

Assuming stationary conditions and a spatially uniform downwind wave field, $F_+ = \text{const}$, the rate of change of the ratio P_-/P_+ is then given by

$$v \frac{\mathrm{d}}{\mathrm{d}r}(P_-/P_+) = \frac{S_-}{F_+}.$$

For a given spectral shape, the non-dimensional growth rate

$$\beta = \lambda \frac{\mathrm{d}}{\mathrm{d}r}(P_-/P_+) = \frac{2}{f} \frac{S_-}{F_+}$$

of the upwind wave components of wavelength λ or frequency f scales theoretically as $\beta = \alpha^2 \times \text{function } (f/f_m)$, where f_m is the frequency scale of the spectrum and α a non-dimensional energy scale. We chose f_m in the following as the peak frequency and α as Phillips' constant (Phillips, 1966).

The growth rate β was computed numerically for the following cases:

(i) *J* JONSWAP spectrum (Hasselmann *et al.*, 1973) with a frequency-independent angular distribution proportional to $\cos^4 \theta/2$, in accordance with the measurements of Tyler *et al.* (1974);

(ii) $J_{1/2}$ JONSWAP spectrum, but with a half-plane frequency-independent angular distribution proportional to $\cos^4 \theta$ for downwind components, $|\theta| < \pi/2$, and zero otherwise; and

(iii) *PM* Pierson–Moskowitz (1964) spectrum with the same angular distribution as J.

In all cases the Phillips' constant was chosen as $\alpha = 0.01$. The computed and observed growth rates are shown in Figure 4. The vertical length of the rectangular box representing the observed data corresponds to the scatter of the growth curves given in Figure 3. The horizontal dimension reflects the variation of wind speeds encountered during the experiment.

The JONSWAP spectrum J gives the best agreement, although the fully developed Pierson–Moskowitz spectrum is probably more relevant for the present geometry. The half-plane angular distribution in the case $J_{1/2}$ is shown primarily for comparison and is probably less realistic than the full-plane $\cos^4 \theta/2$ angular distributions in cases J and PM, which correspond to actual measurements by Tyler *et al.* (1974). The difference by two orders of magnitude between cases J and $J_{1/2}$ illustrates the sensitivity of the results to the directional distribution. The computed energy transfer has the characteristics of a narrow-angle scattering process, with very little energy transfer into regions in the wave-number plane far removed from regions of significant energy (see Figure 5). This results in a strong sensitivity of the upwind growth rate on the level of the spectrum near $\theta = \pm\pi/2$, with the half-plane $\cos^4 \theta$ distribution yielding small growth rates because the spreading function approaches zero rather rapidly as $\theta \to \pm\pi/2$. Narrow-angle scattering also explains the two orders of magnitude difference between the downwind and upwind transfer rates in Figure 4.

No single spectral model can be applicable throughout the full fetch range, since the directional distribution will change with increasing upwind fetch, as noted by one of the reviewers of this paper. Immediately at the shore, the spreading function is identically zero in the upwind direction (ignoring the reflection of downwind waves), but with increasing fetch, the upwind angular distribution will gradually fill in from the sides. The full-plane $\cos^4 \theta/2$ distribution is probably most applicable for large fetches, whereas for small fetches a half-plane angular distribution with discontinuities at $\theta = \pm\pi/2$ may be expected. The latter distribution is not included in the examples given, but computations for a half-plane $\cos^4 \theta/2$ angular distribution, containing a discontinuity at $\theta = \pm\pi/2$, for a Pierson–Moskowitz frequency spectrum, yielded growth rates essentially identical to the curve PM-a in Figure 4 in the range $0.5 < f/f_m < 1.5$.

Curves 'a' in Figure 4 differ from curves 'b' by including only the positive lobe of the growth curve in the upwind half-plane. As the upwind directional distribution

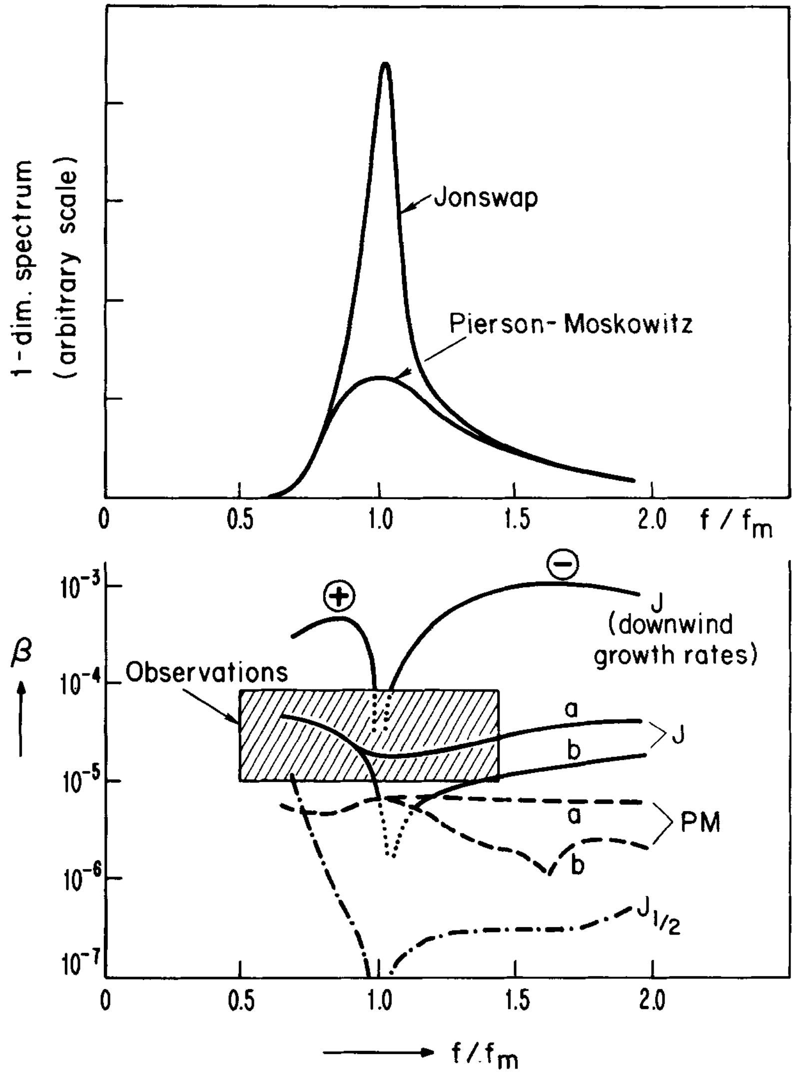

Fig. 4. *Upper panel*: JONSWAP and Pierson–Moskowitz spectra. *Lower panel*: Growth parameter $\beta = (2/f)(S_-/F_+)$ of upwind travelling waves for the cases: J – JONSWAP spectrum with $\cos^4(\theta/2)$ spreading factor; $J_{1/2}$ – JONSWAP spectrum with $\cos^4\theta$ half-plane spreading factor; PM – Pierson–Moskowitz spectrum with $\cos^4(\theta/2)$ spreading factor. The branches (b) represent the net growth in the full upwind half plane. The branches (a) include only upwind components with positive growth rates (see Figure 5). The uppermost curves show for comparison the corresponding growth rate $|(2/f)(S_+/F_+)|$ for downwind travelling waves ($\oplus$ denotes growth, $\ominus$ decay).

fills in, the negative lobes which develop near $\theta = \pm\pi/2$ tend to cancel the positive growth rates for angles closer to the upwind direction; see Figure 5. This may be the explanation for the flattening of the growth curves at large fetches.

A more accurate analysis of the evolution of the directional distribution with fetch clearly requires a full integration of the transport equation for an evolving

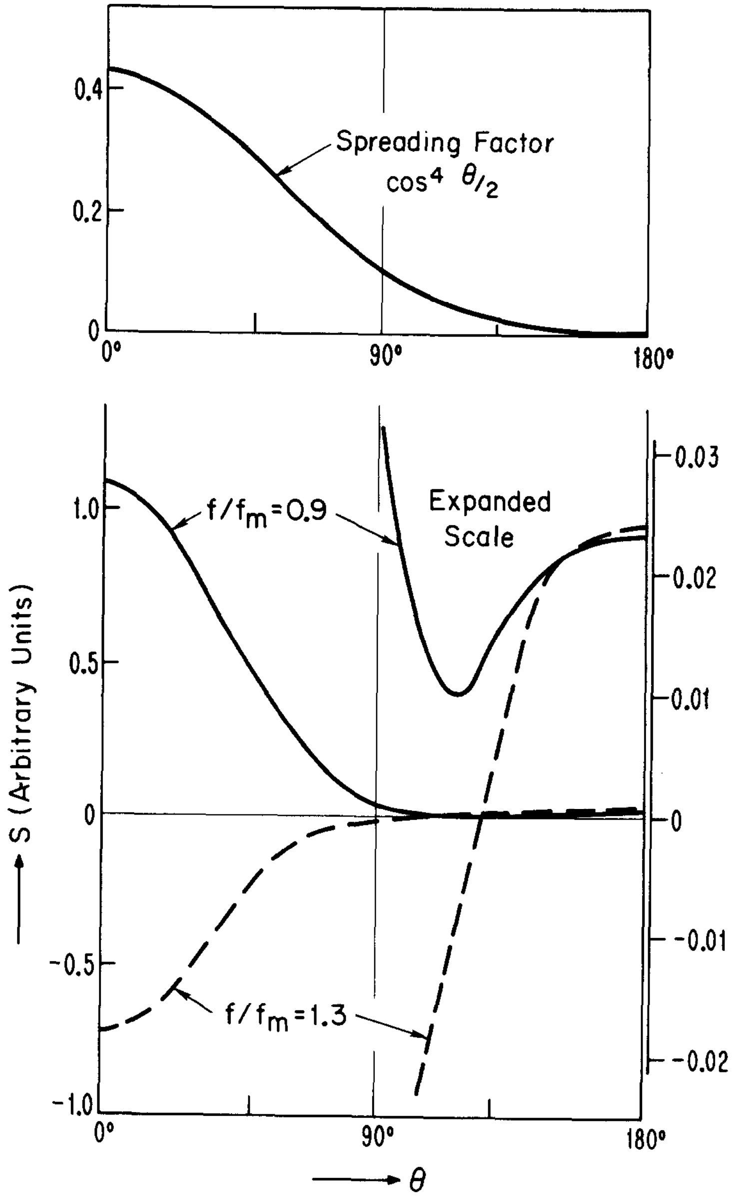

Fig. 5. Directional distribution of energy transfer S for case J for a frequency $f = 0.9\,f_m$ on the forward face of the spectrum and a frequency $f = 1.3\,f_m$ beyond the peak. The growth rates in the upwind half plane are generally two orders of magnitude lower than the transfer rate in the downwind half plane.

spectrum rather than computations of the local transfer rates for selected spectra. However, from the examples given, it appears that the non-linear energy transfer in the upwind half-plane is at least of the general order of magnitude needed to explain the observed upwind growth rates.

4. Conclusions

Computations of the rates of growth of upwind travelling waves generated by non-linear wave–wave interactions show general order of magnitude agreement with the growth rates determined from HF backscatter measurements.

Although a more detailed quantitative comparison was not possible with the present instrumentation owing to the limited half-plane directional resolution, it appears probable that non-linear interactions are the principal source of the upwind travelling waves which have been observed in a number of recent experiments.

References

Barrick, D. E., Headrick, J. M., Bogle, R. W., and Crombie, D. D.: 1974, 'Sea Backscatter at HF: Interpretation and Utilization of the Echo', *Proc. IEE* **62**, 673–680.

Crombie, D. D.: 1971, 'Backscatter of HF Radio Waves from the Sea', in J. R. Wait (ed.), *Electromagnetic Probing in Geophysics*, Golem Press, Boulder, Colorado, Chap. 4.

Crombie, D. D.: 1972, 'Resonant Backscatter from the Sea and Its Application to Physical Oceanography', *Proc. 1972 IEEE Conf. Engineering in the Ocean Environment.*

Fox, M. J. H.: 1976, 'On the Nonlinear Transfer of Energy in the Peak of a Gravity-Wave Spectrum II', *Proc. Roy. Soc.* **A. 348** (1655), 467–483.

Hasselmann, K.: 1962, 'On the Non-Linear Energy Transfer in a Gravity-Wave Spectrum. I: General Theory', *J. Fluid Mech.* **12**, 481–500.

Hasselmann, K.: 1963a, 'On the Non-Linear Energy Transfer in a Gravity-Wave Spectrum. 2: Conservation Theorems, Wave-Particle Correspondence, Irreversibility', *J. Fluid Mech.* **15**, 273–281.

Hasselmann, K.: 1963b, 'On the Non-Linear Energy Transfer in a Gravity-Wave Spectrum. 3: Computation of the Energy Flux and Swell-Sea Interactions for a Neumann Spectrum', *J. Fluid Mech.* **15**, 385–398

Hasselmann, K., Barnett, T. P., Bouws, E., Carlson, H., Cartwright, D. E., Enke, K., Ewing, J. A., Gienapp, H., Hasselmann, D. E., Kruseman, P., Meerburg, A., Müller, P., Olbers, D. J., Richter, K., Sell, W., and Walden, H.: 1973, 'Measurement of Wind-Wave Growth and Swell Decay during the Joint North Sea Wave Project (JONSWAP)', *Deutsche Hydrographische Zeitschrift Suppl.* **A8° (12)**, 1–95.

Herterich, K. and Hasselman, K.: 1977, 'A Similarity Relation for the Nonlinear Energy Transfer in a Finite-Depth Gravity-Wave Spectrum', (submitted for publication).

Longuet-Higgins, M. S.: 1962, 'Resonant Interactions Between Two Trains of Gravity Waves', *J. Fluid Mech.* **12**, 138–159.

Longuet-Higgins, M. S.: 1975, 'On the Nonlinear Transfer of Energy in the Peak of a Gravity-Wave Spectrum', *Proc. Roy. Soc. Lond.* **A. 347**, 311.

Phillips, O. M.: 1960, 'On the Dynamics of Unsteady Gravity Waves of Finite Amplitude. Part I', *J. Fluid Mech.* **9**, 193–217.

Phillips, O. M.: 1966, *The Dynamics of the Upper Ocean*, Cambridge University Press.

Pierson, W. J., Jr. and Moskowitz, L.: 1964, 'A Proposed Spectral Form for Fully Developed Wind Seas Based on the Similarity Theory of S. A. Kitaigorodskii', *J. Geophys. Res.* **69**, 5181–5190.

Sell, W. and Hasselmann, K.: 1972, 'Computations of Nonlinear Energy Transfer for JONSWAP and Empirical Wind Wave Spectra', (Report), Institute of Geophysics, University of Hamburg.

Snyder, R. L.: 1974, 'A Field Study of Wave-Induced Pressure Fluctuations above Surface Gravity Waves', *J. Marine Res.* **32**, 497–531.

Tyler, G. L., Teague, C. C., Stewart, R. H., Peterson, A. M., Munk, W. H., and Joy, J. W.: 1974, 'Wave Directional Spectra from Synthetic Aperture Observations of Radio Scatter', *Deep-Sea Res.* **21**, 989–1016.

Webb, D. J.: 1977, 'Non-Linear Transfers Between Sea Waves', (Unpublished Manuscript).